

RHIC $\sqrt{s_{NN}} = 200$ GeV hadron yields and the isospin dependent equation of state

Feyisola Nana,¹ Jordi Salinas San Martín,¹ and Jacquelyn Noronha-Hostler¹

¹*Illinois Center for Advanced Studies of the Universe, Department of Physics,
University of Illinois at Urbana-Champaign, Urbana, IL 61801, USA*

The statistical hadronization model has been successful in extracting information at chemical freeze-out in heavy-ion collisions. At RHIC, with a collision energy of $\sqrt{s_{NN}} = 200$ GeV, many different ion species have been used for $A+A$ collisions. This allows for a scan across the charge fraction $Y_Q = Z/A$, where Z is the proton number and A is the baryon number. We first make predictions for $A+A$ collisions that do not yet have published experimental data on hadron yield ratios (O+O, Ru+Ru, Zr+Zr). We then use both the experimental and predicted yield ratios to perform thermal fits across Y_Q , enabling us to extract s/n_B and other thermodynamic information at chemical freeze-out. Using the relation between s/n_B and Y_Q , we can calculate a new constraint on the finite temperature equation of state at finite densities. We discuss implications of this constraint and propose future runs that can help connect to the equation of state relevant for neutron star mergers.

Introduction.—Heavy-ion collisions at the relativistic heavy-ion collider (RHIC) explore the Quantum Chromodynamics (QCD) phase diagram at high temperatures T and a range of baryon densities n_B . In the early stages of these collisions, the quark gluon plasma (QGP) is produced. It then expands and cools until the quarks and gluons within the QGP eventually hadronize, and the newly produced particles freeze-out. At the point of freeze-out, it is assumed that the fireball is at chemical equilibrium such that one can use a statistical hadronization model (SHM) [1–13] to extract the temperature and chemical potentials for a specific beam energy $\sqrt{s_{NN}}$ and colliding species containing A nucleons and Z protons using so-called thermal fits.

From QCD there are three conserved charges in heavy-ion collisions: baryon number (B), strangeness (S), and electric charge (Q). While local fluctuations of BSQ charge densities exist [14, 15], globally the system remains strange-neutral throughout the evolution such that the global *average* strangeness density is zero,

$$\langle n_S \rangle = 0. \quad (1)$$

Since both electric charge and baryon number are conserved, the ratio of charge fraction (average electric charge density over the average baryon density)

$$Y_Q \equiv \frac{Z}{A} = \frac{\langle n_Q \rangle}{\langle n_B \rangle} \quad (2)$$

is globally conserved as well. Thus, given a specific ion species, Y_Q is defined for the system and conserved throughout the entire evolution. To date, experiments at RHIC have covered a wide set of species with a significant range of $Y_Q = [0.387, 0.5]$ for a collision energy of $\sqrt{s_{NN}} = 200$ GeV, as shown in Table I [16–18]. Equations (1-2) define the *strangeness neutrality* and *charge fraction conservation* conditions. By applying these conditions, the phase space of $\{T, \mu_B, \mu_S, \mu_Q\}$ can be constrained so that our equation of state simplifies to a function of

just $\{T, \mu_B\}$. The other chemical potentials are then functions of T and μ_B , specifically $\mu_S = \mu_S(T, \mu_B)$ and $\mu_Q = \mu_Q(T, \mu_B)$. With these constraints, one can calculate thermodynamic quantities at the point of freeze-out, such as energy density ε and entropy over the baryon density, s/n_B [19–22].

System	Z	A	Y_Q	Published yield data?
O+O	8	16	0.500	no
Cu+Cu	29	63	0.460	yes
Ru+Ru	44	96	0.458	no*
Zr+Zr	40	96	0.417	no*
Au+Au	79	198	0.399	yes
U+U	92	238	0.387	yes

* Preliminary data has recently been presented in Ref. [23].

TABLE I. Collision systems for heavy-ion experiments at approximately $\sqrt{s_{NN}} = 200$ GeV with their corresponding proton number, atomic mass, charge fraction, and data availability status for hadron yield ratios of identified charged particles.

While heavy-ion collisions probe (approximately) symmetric nuclear matter, neutron star mergers can only be described via isospin dependent equations of state [24–41]. It has recently been pointed out in Ref. [42] that the dense matter equation of state, can be explored through a well-defined expansion up to second order in T for $(T/\mu_B) \ll 1$. This expansion can be cast in terms of derivatives of s/n_B with respect to temperature and the isospin asymmetry parameter defined by

$$\delta \equiv 1 - 2Y_Q, \quad (3)$$

namely,

$$\left. \frac{\partial(s/n_B)}{\partial T} \right|_{\delta=0, T=0}, \quad \left. \frac{\partial^3(s/n_B)}{\partial \delta^2 \partial T} \right|_{\delta=0, T=0}.$$

The number of different colliding systems that have been run at RHIC at $\sqrt{s_{NN}} = 200$ GeV open the possibility to

extract the derivative

$$\left. \frac{\partial^2(s/n_B)}{\partial \delta^2} \right|_{\delta=0, T=\text{const.}}, \quad (4)$$

from heavy-ion data at a fixed point in $\{T, \mu_B, \mu_S\}$ (μ_Q , of course, varying with δ). In principle, if multiple ions were run at other beam energies, we could then extract the dependence of this derivative on T, μ_B , and μ_S as well. Currently, hadron yield data does not yet exist for all the species listed in Table I. Extensive data exist for Au+Au [17] at $\sqrt{s_{NN}} = 200$ GeV for 0–5% centrality, with a smaller subset of data available for U+U [18] at $\sqrt{s_{NN}} = 197$ GeV for 0–5% centrality, and for Cu+Cu [16] at $\sqrt{s_{NN}} = 200$ GeV for 0–10% centrality. To be consistent across systems, we limit ourselves to yield ratios of identified charged particles where data exist for all three ion pairs. While Zr+Zr, Ru+Ru, and O+O have all been run experimentally, the hadron yield ratio data have not yet been published for these species.

In this Letter, we first develop a method to predict the hadron yield ratios of these species based on the available knowledge from Cu+Cu, Au+Au, and U+U. Then, using a combination of our predicted hadron yield ratios and the existing ratios, we are able to calculate the derivative in Eq. (4) and comment on its implication for the dense matter equation of state. We confirm that T, μ_B , and μ_S are nearly constant for a fixed collision energy while we vary Y_Q . We then determine that the derivative is $\left. \frac{\partial^2(s/n_B)}{\partial \delta^2} \right|_{\delta=0, T \approx 145 \text{ MeV}} = -0.183_{-0.166}^{+0.128} \times 10^5$. We propose future runs that can provide further insight into the dense matter equation of state relevant to neutron star mergers.

Estimating hadron yield ratios.—One of the most successful statistical models used to describe strongly interacting matter in the hadronic phase is the Hadron Resonance Gas (HRG) model. This model represents hadrons using the grand canonical ensemble (GCE) framework. The basic quantity required to compute thermodynamic properties and the thermal composition of the particle (hadron) yields measured in relativistic heavy-ion collisions is the partition function $\mathcal{Z}(T, V)$ [4]. Within a strongly interacting medium where the three conserved charges are included, the GCE partition function can be written as a sum over all known hadrons and resonances listed in the Review of Particle Physics by the Particle Data Group (PDG),

$$\ln \mathcal{Z}_{\text{HRG}}(T, V, \vec{\mu}) = \sum_{i \in \text{PDG}} \ln \mathcal{Z}_i(T, V, \vec{\mu}), \quad (5)$$

where

$$\ln \mathcal{Z}_i(T, V, \vec{\mu}) = \pm \frac{g_i V}{2\pi^2} \int_0^\infty p^2 dp \ln \left[1 \pm e^{-(E_i - \mu_i)/T} \right] \quad (6)$$

is the partition function of the i -th particle, $\vec{\mu} = (\mu_B, \mu_S, \mu_Q)$ represents the chemical potentials associated with the conserved charges, $\mu_i = (B_i \mu_B + S_i \mu_S + Q_i \mu_Q)$, the total energy is $E_i = \sqrt{p^2 + m_i^2}$ for a particle with mass m_i , and $g_i = (2J_i + 1)$ is the spin degeneracy factor. The positive sign corresponds to fermions, and the negative sign to bosons. By performing the momentum integration in Eq. 6, one can analytically determine the total pressure as well as other thermodynamic quantities such as the particle number density n_i , entropy density s_i , and energy density ε_i :

$$n_i(T, \mu_i) = \frac{T}{V} \left(\frac{\partial \ln \mathcal{Z}_i}{\partial \mu_i} \right)_{T, V} = \frac{g_i}{2\pi^2} \int_0^\infty \frac{p^2 dp}{\exp[(E_i - \mu_i)/T] \pm 1}, \quad (7)$$

$$\varepsilon_i(T, \mu_i) = -\frac{1}{V} \left(\frac{\partial \ln \mathcal{Z}_i}{\partial (1/T)} \right)_{\mu_i/T, V} = \frac{g_i}{2\pi^2} \int_0^\infty \frac{p^2 E_i dp}{\exp[(E_i - \mu_i)/T] \pm 1}, \quad (8)$$

$$s_i(T, \mu_i) = \frac{1}{V} \left(\frac{\partial (T \ln \mathcal{Z}_i)}{\partial T} \right)_{\mu_i, V} = \pm \frac{g_i}{2\pi^2} \int_0^\infty p^2 dp \left(\ln (1 \pm \exp[-(E_i - \mu_i)/T]) \pm \frac{E_i - \mu_i}{T (\exp[(E_i - \mu_i)/T] \pm 1)} \right). \quad (9)$$

We study the following ratios of hadronic yields: π^-/π^+ , K^-/K^+ , \bar{p}/p , K^-/π^- , and \bar{p}/π^- rather than yields, to minimize system size effects¹. The summary of

the ratios used and their experimental values can be found in Table II. Additionally, some of the systematic uncertainties cancel when studying ratios (as compared to yields), since both particles in each ratio are detected under the same experimental conditions. Most of the available experimental data do not account for the contribution of feed-down from weak decays, mainly affecting the (anti)proton

¹ Data also exist for K^+/π^+ and p/π^+ , but these are redundant given the other ratios available, so we exclude it from our fits.

Ratio	Cu+Cu [16]	Au+Au [17]	U+U [18]
π^-/π^+	1.003 ± 0.050	1.015 ± 0.051	1.005 ± 0.056
K^-/K^+	0.936 ± 0.051	0.965 ± 0.048	0.938 ± 0.066
\bar{p}/p (uncorr.)	0.801 ± 0.040	0.769 ± 0.055	0.758 ± 0.074
\bar{p}/p (corr.)	0.771 ± 0.038	0.740 ± 0.053	0.729 ± 0.071
K^-/π^-	0.144 ± 0.016	0.151 ± 0.018	0.145 ± 0.020
\bar{p}/π^- (uncorr.)	0.077 ± 0.008	0.082 ± 0.010	0.077 ± 0.012
\bar{p}/π^- (corr.)	0.0489 ± 0.0051	0.0521 ± 0.0063	0.0489 ± 0.0076

TABLE II. Experimentally measured hadron yield ratios and corresponding error of identified charged particles in Cu+Cu, Au+Au, and U+U collision systems. STAR collaboration data at $\sqrt{s_{NN}} = 200$ GeV for Cu+Cu and Au+Au; in the case of U+U, data from the $\sqrt{s_{NN}} = 197$ GeV run is provided. Feed-down contributions are included.

yields. Following the estimations from Refs. [6, 43], our model corrects for this contribution by scaling the proton and antiproton yields by 66% and 63.5%, respectively, assuming an even correction across collision systems. Using these ratios, we perform a minimum χ^2 fit using THERMAL-FIST [13] to obtain $\{T, \mu_B, \mu_S, \mu_Q\}$ at chemical freeze-out, given the strangeness neutrality condition and the electric-to-baryon charge ratio Y_Q .

To predict the yield ratios for species whose experimental runs have been completed but not yet published, we fit various functional forms to the available data, incorporating the error bars from existing experimental results. This approach allows us to estimate the yield ratios and associated uncertainties for O+O, Ru+Ru, and Zr+Zr systems as a function of Y_Q by interpolating or extrapolating, as necessary. The fitted functional forms are polynomials of first-, second-, and third-orders:

$$p_m(Y_Q) = \sum_{i=0}^m a_{m,i} Y_Q^i; \quad m = \{1, 2, 3\}, \quad (10)$$

where we vary the coefficients $a_{m,i}$ within a specified range (see Table IV) and eliminate fits that do not fall within the given error bars².

In Fig. 1 we show the results of our fits for each of the different yield ratios as functions of Y_Q . Both the experimental data points (Cu+Cu, Au+Au, U+U) and predicted yield ratios (O+O, Ru+Ru, Zr+Zr) with errors are shown. In addition to the experimental constraints, since O+O collisions should produce precisely symmetric nuclear matter ($Y_Q = 0.5$), we set the π^-/π^+ yield ratio to exactly unity. We summarize our results for the predicted yield ratios for O+O, Ru+Ru, and Zr+Zr in Table III.

The predicted yield ratios for Ru+Ru and Zr+Zr are generally well estimated, with error bars comparable in size to the experimental data points (Ru+Ru is especially well constrained because its Y_Q is nearly identical

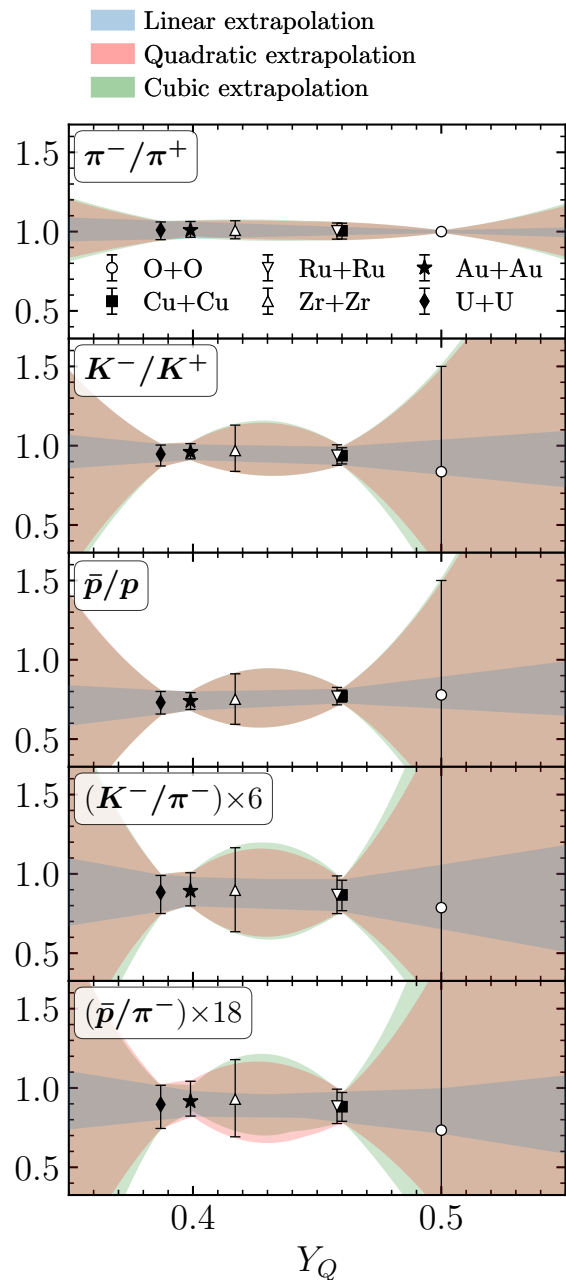


FIG. 1. Charge fraction dependence of hadron yield ratios. Experimental data points (closed symbols) for Cu+Cu [16], Au+Au [17], U+U [18] results and predicted ratios (open symbols) for O+O, Ru+Ru, and Zr+Zr collision systems. The large error band for O+O is a result of its $Y_Q = 0.5$ being outside the regime of validity. K^-/π^- are rescaled by 6 and \bar{p}/π^- by 18. Feed-down contributions are included.

to Cu+Cu). Although the K^-/π^- and p/π^- ratios have slightly larger error bars, actual experimental measurements will help to reduce this uncertainty. However, O+O collisions have significantly larger uncertainties. The O+O error arises because its charge fraction, $Y_Q = 0.5$, falls outside the range of experimental Y_Q values being con-

² The code used to perform this analysis can be found: https://github.com/jordissm/YQ_InterpolatorAndExtrapolator.git

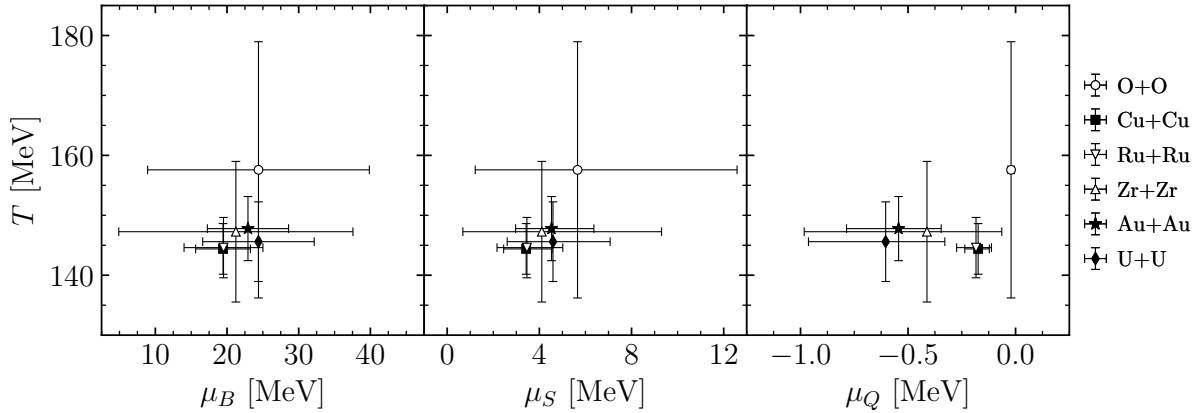


FIG. 2. The QCD phase diagram $T-\mu_{B,S,Q}$ planes at chemical freeze-out extracted from $\sqrt{s} = 200$ GeV. The predicted ratios are marked by the open symbols while closed symbols indicate ratios of the fits from experimental data.

Ratio	O+O	Ru+Ru	Zr+Zr
π^-/π^+	1.000	1.003 ± 0.051	1.011 ± 0.057
K^-/K^+	0.781 ± 0.781	0.941 ± 0.065	0.984 ± 0.146
\bar{p}/p (uncorr.)	0.780 ± 0.780	0.801 ± 0.057	0.782 ± 0.165
\bar{p}/p (corr.)	0.750 ± 0.750	0.771 ± 0.055	0.752 ± 0.159
K^-/π^-	0.187 ± 0.187	0.145 ± 0.020	0.150 ± 0.044
\bar{p}/π^- (uncorr.)	0.098 ± 0.098	0.077 ± 0.009	0.082 ± 0.021
\bar{p}/π^- (corr.)	0.0625 ± 0.0625	0.0491 ± 0.0060	0.0520 ± 0.0135

TABLE III. Predicted hadron yield ratios and corresponding error of identified charged particles in O+O, Ru+Ru, and Zr+Zr collision systems at $\sqrt{s_{NN}} = 200$ GeV. Both corrected and uncorrected results for feed-down contributions are shown.

sidered $Y_Q = [0.387, 0.460]$ and it is therefore difficult to extrapolate beyond the regime of validity. In contrast, the π^-/π^+ yield ratio estimations have small uncertainties across the entire range of charge fractions considered, due to the additional constraint on symmetric nuclear matter. Thus, of the three nuclei for which we have predicted yield ratios using the known experimental yield ratios, the experimental data for the yield ratios from O+O collisions should provide the most important constraints.

Now that we have yield ratios across the range $Y_Q = [0.387, 0.5]$ from both the experimental data and theoretical predictions, we can use them to extract the thermodynamic information at chemical freeze-out. To do so, we use the hadron resonance gas model from the THERMAL-FIST [13] package. Within THERMAL-FIST, one can perform a minimum χ^2 fit to the experimental yield ratios (see Appendix A for further details) using the most up-to-date hadronic list (PGD2021+) [44]. The output is then the freeze-out parameters $\{T^{\text{FO}}, \mu_B^{\text{FO}}, \mu_S^{\text{FO}}, \mu_Q^{\text{FO}}\}$ for each Y_Q . Once $\{T^{\text{FO}}, \mu_B^{\text{FO}}, \mu_S^{\text{FO}}, \mu_Q^{\text{FO}}\}$ along Y_Q are known, we can then insert these values into the HRG calculations of the equation of state to determine the relevant thermodynamic quantities such as s/n_B , energy density ε , and the baryon density in terms of the saturation density n_B/n_{sat} .

We limit our analyses to the default thermal fits: ideal non-interacting gas model, grand canonical ensemble, and energy-independent Breit-Wigner resonance widths, while varying the thermal configurations for the different Y_Q values.

Discussion.—In Fig. 2 we show our resulting values for $\{T^{\text{FO}}, \mu_B^{\text{FO}}, \mu_S^{\text{FO}}, \mu_Q^{\text{FO}}\}$ for different ion species, i.e., different values of Y_Q . The freeze-out temperatures are nearly identical across Y_Q , as one would expect. Generally, the values for $\{T^{\text{FO}}, \mu_B^{\text{FO}}\}$ and $\{T^{\text{FO}}, \mu_S^{\text{FO}}\}$ for different ion species overlap within the error bars for all Y_Q . The O+O predictions have significantly larger error bars due to extrapolation issues. However, the results of $\{T^{\text{FO}}, \mu_Q^{\text{FO}}\}$ do not all overlap at freeze-out. Because O+O collisions produce exactly symmetric nuclear matter, $\mu_Q = 0$ by definition. We find that the ordering of μ_Q values—starting with the most negative: U+U, Au+Au, Zr+Zr, Ru+Ru, Cu+Cu, O+O—is consistent with their ordering in Y_Q , even though some error bars are still large.

Using the freeze-out parameters $\{T^{\text{FO}}, \mu_B^{\text{FO}}, \mu_S^{\text{FO}}, \mu_Q^{\text{FO}}\}$, we can calculate the relevant thermodynamic quantities as functions of Y_Q . In Fig. 3 we show the energy density versus Y_Q (top), the baryon number density versus Y_Q (middle), and the entropy per baryon number versus Y_Q (bottom). Most relativistic hydrodynamic models choose a fixed energy density at freeze-out [15, 45–47], from our results here we find that $\varepsilon^{\text{FO}}(Y_Q) \approx \text{const.}$ such that a constant energy density approach is a good assumption at least across Y_Q . Next, we compare the baryon density in terms of n_{sat} where we assume $n_{\text{sat}} = 0.16 \text{ fm}^{-3}$. Given the current error bars in our results, $n_B(Y_Q)$ may either be constant or exhibit a slightly inverse scaling relation with Y_Q . However, systems with smaller Y_Q also correspond to larger systems, increasing the probability of baryon stopping. With the given data we cannot delve deeper into this effect but leave it as a future topic when more experimental data becomes available. Finally, we observe

the change in $s/n_B(Y_Q)$. In Ref. [42], it was found using a relativistic mean-field model at a low constant temperature that s/n_B decreases with decreasing Y_Q (although $s/n_B(Y_Q)$ remained fairly flat for Y_Q close to 0.5), which is consistent with our findings. What was most pertinent to constrain the development of 3-dimensional equations of state for neutron star mergers is the derivative shown in Eq. (4) wherein we have rewritten Y_Q in terms of δ defined in Eq. (3). Using our results in Fig. 3 (bottom), we fit polynomial functional forms to $s/n_B(Y_Q)$ within the error bars to compute the needed derivative. Because we require a second-order derivative, these functional forms must be at a least quadratic functions to obtain a non-zero result. Thus, we fit only quadratic and quartic forms to our results for $s/n_B(Y_Q)$.

The results of $\partial^2(s/n_B)/\partial\delta^2$ are shown in Fig. 4 wherein we plot it versus δ . This derivative should be taken at a $T = \text{const.}$, which is reasonable given Fig. 2 where $T^{\text{FO}} \approx 145$ MeV for all ion species considered. For the neutron star merger equation of state, one would also want to take the $\delta \rightarrow 0$ limit, which is somewhat more challenging because our O+O results are predictions and not experimental data. Therefore, we argue that the O+O yield ratio results are crucial not only for constraining the hadron yield ratios but also for taking the $\delta \rightarrow 0$ limit. Overall, the result of $\partial^2(s/n_B)/\partial\delta^2$ is in qualitative agreement with what was found in Fig. 6 of Ref. [42]. However, ideally, we would have results across multiple different T , n_B , and δ to reconstruct this derivative across a wider region of the phase diagram.

Conclusions and outlook.—In this paper we use existing hadron yield ratios at top RHIC energies to make predictions for the yield ratios of O+O, Ru+Ru, and Zr+Zr. Then we extract thermodynamic quantities at freeze-out across a range in Y_Q . From our analysis, we are able to provide new insights into the effect of Y_Q on the equation of state. We find that the assumption of $\varepsilon = \text{const.}$ at freeze-out appears to be a good assumption as one changes $Y_Q = Z/A$ of the colliding ions. We find that the ratio of s/n_B increases with Y_Q such that if one calculates the second derivative of s/n_B at fixed T with respect to δ we obtain a negative derivative, which is consistent with theoretical calculations [32] in the regime relevant to neutron star mergers [42]. Finally, we find that experimental hadron yield results for O+O would be the most informative because we require experimental data for symmetric nuclear matter.

Our results demonstrate the importance of having hadron yield ratio data across a wide range of $Y_Q = Z/A$ (different choice of colliding species) and different T and μ_B (different choice of $\sqrt{s_{NN}}$). Potential ions of interest that are both stable and provide useful Y_Q values are: ${}^3\text{He}$ with $Y_Q \approx 0.66$, ${}^7\text{Be}$ with $Y_Q \approx 0.57$, ${}^{40}\text{Ca}$ or ${}^{44}\text{Ti}$ with $Y_Q = 0.50$, ${}^{58}\text{Ni}$ with $Y_Q \approx 0.483$, and ${}^{96}\text{Mo}$ of $Y_Q \approx 0.434$. Another interesting possibility to reach even lower values in Y_Q is the use unstable beams. Further runs

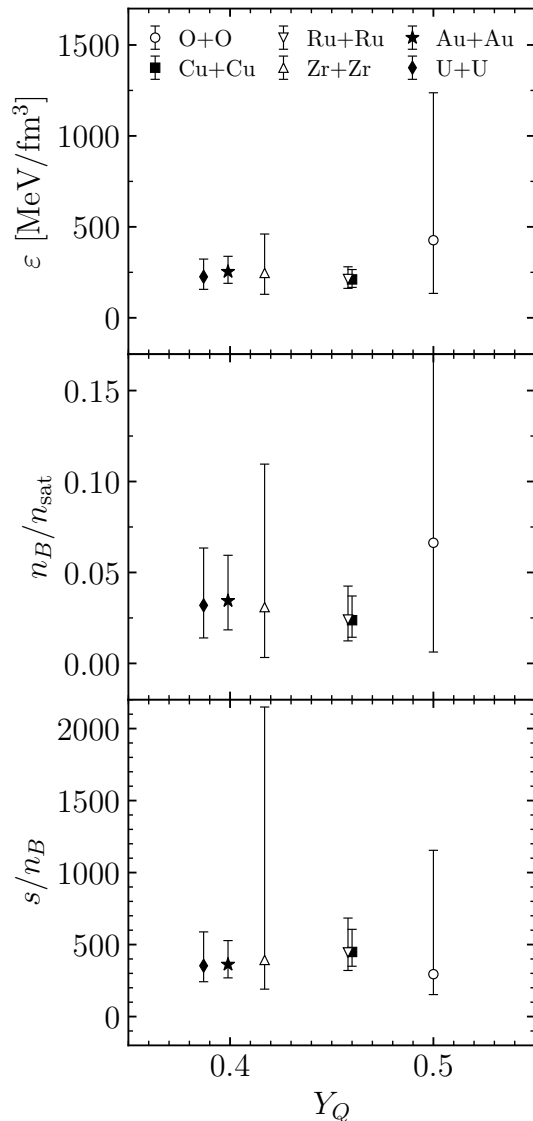


FIG. 3. Charge fraction dependence of the energy density (top), baryon number density in terms of n_{sat} (middle), and entropy per baryon number (bottom). Closed symbols are extracted from experimental data, open symbols are extracted from predictions for yield ratios.

using distinct colliding ion species across different $\sqrt{s_{NN}}$ would allow us to calculate the second derivative of s/n_B with respect to δ , essential to constraining the equation of state of neutron star mergers. Low collision energies would be ideal to access information at large μ_B and lower T . While the STAR experiment has already finished its Beam Energy Scan runs, there is still an opportunity to run scans in Y_Q and $\sqrt{s_{NN}}$ in the upcoming Compressed Baryonic Matter (CBM) at FAIR [48]. Additionally, it would also be interesting to conduct a similar Y_Q scan at the LHC, which will eventually be possible using ${}^{208}\text{Pb}$, ${}^{129}\text{Xe}$, ${}^{16}\text{O}$ that translate to $Y_Q = 0.39, 0.42, 0.5$, respec-

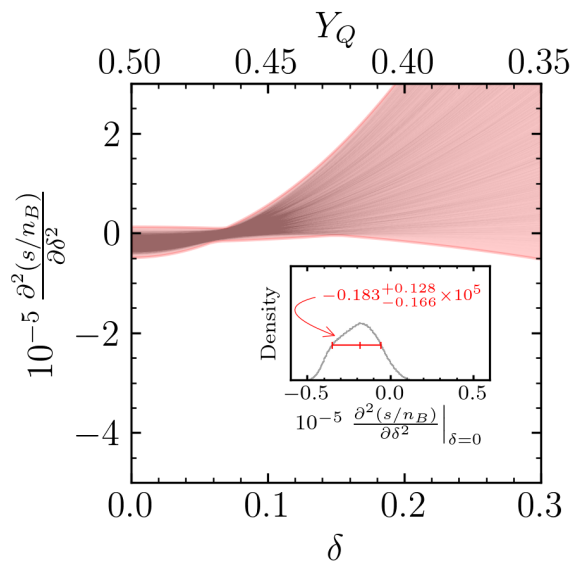


FIG. 4. Second derivative of s/n_B with respect to the isospin asymmetry parameter δ calculated from polynomial fits for the isentrope values extracted from thermal fits. The area bounding all possible quartic polynomials that fit data is shown in red, and a subset of the second derivative of these polynomials is depicted by gray lines. (Inset) Histogram of all resulting polynomials in the limit $\delta \rightarrow 0$; result in red marks the value of the second derivative at the peak of the distribution and the uncertainty is fixed where the distribution falls $e^{-1/2}$ from the peak.

tively. Combining our results here with an LHC scan in Y_Q would then allow us to construct the $\partial^2(s/n_B)/\partial\delta^2$ derivatives at two different points in μ_B for a nearly constant T . Future Y_Q scans could also provide insight to the kaon isospin anomaly [49–51] and the disorientated isospin condensate [52, 53].

Acknowledgements.—The authors would like to thank D. Mroczek for useful discussions during the preparation of this manuscript. The authors also thank P. Tribedy, R. Ma, and C.Y. Tsang for their comments on recent experimental data. The authors acknowledge support from the US-DOE Nuclear Science Grant No. DE-SC0023861, and within the framework of the Saturated Glue 34 (SURGE) Topical Theory Collaboration. This work was also supported in part by the National Science Foundation (NSF) within the framework of the MUSES collaboration, under grant number OAC-2103680 and from the Illinois Campus Cluster, a computing resource that is operated by the Illinois Campus Cluster Program (ICCP) in conjunction with the National Center for Supercomputing Applications (NCSA), and which is supported by funds from the University of Illinois at Urbana-Champaign.

- [1] R. Dashen, S.-K. Ma, and H. J. Bernstein, S Matrix formulation of statistical mechanics, *Phys. Rev.* **187**, 345 (1969).
- [2] J. Cleymans and K. Redlich, Chemical and thermal freeze-out parameters from 1-A/GeV to 200-A/GeV, *Phys. Rev. C* **60**, 054908 (1999), arXiv:nucl-th/9903063.
- [3] P. Braun-Munzinger, D. Magestro, K. Redlich, and J. Stachel, Hadron production in Au - Au collisions at RHIC, *Phys. Lett. B* **518**, 41 (2001), arXiv:hep-ph/0105229.
- [4] P. Braun-Munzinger, K. Redlich, and J. Stachel, Particle production in heavy ion collisions, in *Quark-Gluon Plasma 3*, pp. 491–599.
- [5] F. Becattini and G. Passaleva, Statistical hadronization model and transverse momentum spectra of hadrons in high-energy collisions, *Eur. Phys. J. C* **23**, 551 (2002), arXiv:hep-ph/0110312.
- [6] A. Andronic, P. Braun-Munzinger, and J. Stachel, Hadron production in central nucleus-nucleus collisions at chemical freeze-out, *Nucl. Phys. A* **772**, 167 (2006), arXiv:nucl-th/0511071.
- [7] J. Cleymans, H. Oeschler, K. Redlich, and S. Wheaton, Comparison of chemical freeze-out criteria in heavy-ion collisions, *Phys. Rev. C* **73**, 034905 (2006), arXiv:hep-ph/0511094.
- [8] S. Wheaton, J. Cleymans, and M. Hauer, THERMUS, (2011), arXiv:1108.4588 [hep-ph].
- [9] A. Andronic, P. Braun-Munzinger, K. Redlich, and J. Stachel, Decoding the phase structure of QCD via particle production at high energy, *Nature* **561**, 321 (2018), arXiv:1710.09425 [nucl-th].
- [10] A. Andronic, P. Braun-Munzinger, B. Friman, P. M. Lo, K. Redlich, and J. Stachel, The thermal proton yield anomaly in Pb-Pb collisions at the LHC and its resolution, *Phys. Lett. B* **792**, 304 (2019), arXiv:1808.03102 [hep-ph].
- [11] A. Andronic, P. Braun-Munzinger, K. Redlich, and J. Stachel, Hadron yields in central nucleus-nucleus collisions, the statistical hadronization model and the QCD phase diagram, in *Criticality in QCD and the Hadron Resonance Gas* (2021) arXiv:2101.05747 [nucl-th].
- [12] J. Cleymans, P. M. Lo, K. Redlich, and N. Sharma, Hadronic Resonance Gas Model and Multiplicity Dependence in p-p, p-Pb, Pb-Pb collisions: Strangeness Enhancement, (2020), arXiv:2010.02714 [hep-ph].
- [13] V. Vovchenko and H. Stoecker, Thermal-FIST: A package for heavy-ion collisions and hadronic equation of state, *Comput. Phys. Commun.* **244**, 295 (2019), arXiv:1901.05249 [nucl-th].
- [14] P. Carzon, M. Martinez, M. D. Sievert, D. E. Wertepny, and J. Noronha-Hostler, Monte Carlo event generator for initial conditions of conserved charges in nuclear geometry, *Phys. Rev. C* **105**, 034908 (2022), arXiv:1911.12454 [nucl-th].
- [15] C. Plumberg *et al.*, BSQ Conserved Charges in Relativistic Viscous Hydrodynamics solved with Smoothed Particle Hydrodynamics, (2024), arXiv:2405.09648 [nucl-th].
- [16] M. M. Aggarwal *et al.* (STAR), Scaling properties at freeze-out in relativistic heavy ion collisions, *Phys. Rev. C* **83**, 034910 (2011), arXiv:1008.3133 [nucl-ex].
- [17] B. I. Abelev *et al.* (STAR), Systematic Measurements of Identified Particle Spectra in pp , d^+ Au and Au+Au

- Collisions from STAR, *Phys. Rev. C* **79**, 034909 (2009), arXiv:0808.2041 [nucl-ex].
- [18] M. S. Abdallah *et al.* (STAR), Pion, kaon, and (anti)proton production in U+U collisions at $\sqrt{s_{NN}}=193$ GeV measured with the STAR detector, *Phys. Rev. C* **107**, 024901 (2023), arXiv:2208.00653 [nucl-ex].
- [19] S. Ejiri, F. Karsch, E. Laermann, and C. Schmidt, The Isentropic equation of state of 2-flavor QCD, *Phys. Rev. D* **73**, 054506 (2006), arXiv:hep-lat/0512040.
- [20] P. Alba, W. Alberico, R. Bellwied, M. Bluhm, V. Mantovani Sarti, M. Nahrgang, and C. Ratti, Freeze-out conditions from net-proton and net-charge fluctuations at RHIC, *Phys. Lett. B* **738**, 305 (2014), arXiv:1403.4903 [hep-ph].
- [21] J. N. Guenther, R. Bellwied, S. Borsanyi, Z. Fodor, S. D. Katz, A. Pasztor, C. Ratti, and K. K. Szabó, The QCD equation of state at finite density from analytical continuation, *Nucl. Phys. A* **967**, 720 (2017), arXiv:1607.02493 [hep-lat].
- [22] C. Ratti, Lattice QCD and heavy ion collisions: a review of recent progress, *Rept. Prog. Phys.* **81**, 084301 (2018), arXiv:1804.07810 [hep-lat].
- [23] R. Ma, Measurements of identified particle spectra in Ru+Ru and Zr+Zr collisions at $\sqrt{s_{NN}} = 200$ GeV by STAR (2024), the 39th Winter Workshop on Nuclear Dynamics.
- [24] B. B. Brandt, G. Endrodi, and S. Schmalzbauer, QCD phase diagram for nonzero isospin-asymmetry, *Phys. Rev. D* **97**, 054514 (2018), arXiv:1712.08190 [hep-lat].
- [25] K. Aryal, C. Constantinou, R. L. S. Farias, and V. Dexheimer, High-Energy Phase Diagrams with Charge and Isospin Axes under Heavy-Ion Collision and Stellar Conditions, *Phys. Rev. D* **102**, 076016 (2020), arXiv:2004.03039 [nucl-th].
- [26] S. Choi, T. Miyatsu, M.-K. Cheoun, and K. Saito, Constraints on Nuclear Saturation Properties from Terrestrial Experiments and Astrophysical Observations of Neutron Stars, *Astrophys. J.* **909**, 156 (2021), arXiv:2011.14557 [nucl-th].
- [27] P. Wen and J. W. Holt, Constraining the nonanalytic terms in the isospin-asymmetry expansion of the nuclear equation of state, *Phys. Rev. C* **103**, 064002 (2021), arXiv:2012.02163 [nucl-th].
- [28] J. P. Carlomagno, D. G. Dumm, and N. N. Scoccola, Isospin asymmetric matter in a nonlocal chiral quark model, *Phys. Rev. D* **104**, 074018 (2021), arXiv:2107.02022 [hep-ph].
- [29] C. Drischler, J. W. Holt, and C. Wellenhofer, Chiral Effective Field Theory and the High-Density Nuclear Equation of State, *Ann. Rev. Nucl. Part. Sci.* **71**, 403 (2021), arXiv:2101.01709 [nucl-th].
- [30] B. S. Lopes, S. S. Avancini, A. Bandyopadhyay, D. C. Duarte, and R. L. S. Farias, Hot QCD at finite isospin density: Confronting the SU(3) Nambu–Jona-Lasinio model with recent lattice data, *Phys. Rev. D* **103**, 076023 (2021), arXiv:2102.02844 [hep-ph].
- [31] J. Liu, C. Gao, N. Wan, and C. Xu, Basic quantities of the equation of state in isospin asymmetric nuclear matter, *Nucl. Sci. Tech.* **32**, 117 (2021), arXiv:2109.11141 [nucl-th].
- [32] M. G. Alford, L. Brodie, A. Haber, and I. Tews, Relativistic mean-field theories for neutron-star physics based on chiral effective field theory, *Phys. Rev. C* **106**, 055804 (2022), arXiv:2205.10283 [nucl-th].
- [33] M. G. Alford, L. Brodie, A. Haber, and I. Tews, Tabulated equations of state from models informed by chiral effective field theory, *Phys. Scripta* **98**, 125302 (2023), arXiv:2304.07836 [nucl-th].
- [34] B. B. Brandt, F. Cuteri, and G. Endrodi, Equation of state and speed of sound of isospin-asymmetric QCD on the lattice, *JHEP* **07**, 055, arXiv:2212.14016 [hep-lat].
- [35] E. R. Most, A. Motornenko, J. Steinheimer, V. Dexheimer, M. Hanauske, L. Rezzolla, and H. Stoecker, Probing neutron-star matter in the lab: Similarities and differences between binary mergers and heavy-ion collisions, *Phys. Rev. D* **107**, 043034 (2023), arXiv:2201.13150 [nucl-th].
- [36] A. Ayala, A. Bandyopadhyay, R. L. S. Farias, L. A. Hernández, and J. L. Hernández, QCD equation of state at finite isospin density from the linear sigma model with quarks: The cold case, *Phys. Rev. D* **107**, 074027 (2023), arXiv:2301.13633 [hep-ph].
- [37] A. Ayala, B. S. Lopes, R. L. S. Farias, and L. C. Parra, On the origin of the peak of the sound velocity for isospin imbalanced strongly interacting matter, (2024), arXiv:2409.19406 [hep-ph].
- [38] A. Sorensen *et al.*, Dense nuclear matter equation of state from heavy-ion collisions, *Prog. Part. Nucl. Phys.* **134**, 104080 (2024), arXiv:2301.13253 [nucl-th].
- [39] R. Kumar *et al.* (MUSES), Theoretical and experimental constraints for the equation of state of dense and hot matter, *Living Rev. Rel.* **27**, 3 (2024), arXiv:2303.17021 [nucl-th].
- [40] T. R. Routray, S. Sahoo, X. Viñas, D. N. Basu, and M. Centelles, Equation of state of hot neutron star matter using finite range simple effective interaction, *J. Phys. G* **51**, 085203 (2024), arXiv:2404.05910 [nucl-th].
- [41] T. Kojo, D. Suenaga, and R. Chiba, Isospin QCD as a Laboratory for Dense QCD, *Universe* **10**, 293 (2024), arXiv:2406.11059 [hep-ph].
- [42] D. Mroczek, N. Yao, K. Zine, J. Noronha-Hostler, V. Dexheimer, A. Haber, and E. R. Most, Finite-temperature expansion of the dense-matter equation of state, (2024), arXiv:2404.01658 [astro-ph.HE].
- [43] F. A. Flor, G. Olinger, and R. Bellwied, Flavour and Energy Dependence of Chemical Freeze-out Temperatures in Relativistic Heavy Ion Collisions from RHIC-BES to LHC Energies, *Phys. Lett. B* **814**, 136098 (2021), arXiv:2009.14781 [nucl-ex].
- [44] J. Salinas San Martin, R. Hirayama, J. Hammelmann, J. M. Karthein, P. Parotto, J. Noronha-Hostler, C. Ratti, and H. Elfner, Thermodynamics of an updated hadronic resonance list and influence on hadronic transport, (2023), arXiv:2309.01737 [nucl-th].
- [45] L. Du, Bulk medium properties of heavy-ion collisions from the beam energy scan with a multistage hydrodynamic model, *Phys. Rev. C* **110**, 014904 (2024), arXiv:2401.00596 [hep-ph].
- [46] W. Zhao, C. Shen, C. M. Ko, Q. Liu, and H. Song, Beam-energy dependence of the production of light nuclei in Au + Au collisions, *Phys. Rev. C* **102**, 044912 (2020), arXiv:2009.06959 [nucl-th].
- [47] D. Almaalol, M. Alqahtani, and M. Strickland, Anisotropic hydrodynamic modeling of 200 GeV Au-Au collisions, *Phys. Rev. C* **99**, 044902 (2019), arXiv:1807.04337 [nucl-th].
- [48] D. Almaalol *et al.*, QCD Phase Structure and Interactions at High Baryon Density: Continuation of BES Physics

Program with CBM at FAIR, (2022), arXiv:2209.05009 [nucl-ex].

- [49] S. Acharya *et al.* (ALICE), Neutral to charged kaon yield fluctuations in Pb – Pb collisions at sNN=2.76 TeV, Phys. Lett. B **832**, 137242 (2022), arXiv:2112.09482 [nucl-ex].
- [50] H. Adhikary *et al.* (NA61/SHINE), Evidence of isospin-symmetry violation in high-energy collisions of atomic nuclei, (2023), arXiv:2312.06572 [nucl-ex].
- [51] W. Brylinski, M. Gazdzicki, F. Giacosa, M. Gorenstein, R. Poberezhnyuk, S. Samanta, and H. Stroebele, Large isospin symmetry breaking in kaon production at high energies, (2023), arXiv:2312.07176 [nucl-th].
- [52] S. Gavin and J. I. Kapusta, Kaon and pion fluctuations from small disoriented chiral condensates, Phys. Rev. C **65**, 054910 (2002), arXiv:nucl-th/0112083.
- [53] J. I. Kapusta, S. Pratt, and M. Singh, Disoriented isospin condensates may be the source of anomalous kaon correlations measured in Pb-Pb collisions at sNN=2.76 TeV, Phys. Rev. C **109**, L031902 (2024), arXiv:2306.13280 [hep-ph].

SUPPLEMENTAL MATERIAL

Thermal Fitting procedure.—In describing the procedure used in our fit, we obtain the best model fit by minimizing the distribution of χ^2 ,

$$\chi^2 \equiv \sum_i \frac{(N_i^{\text{Exp}} - N_i^{\text{HRG}})^2}{\sigma_i^2}, \quad (11)$$

and obtaining an estimate of the systematic error by considering the quadratic deviation Δ^2 defined as:

$$\Delta^2 \equiv \sum_i \frac{(N_i^{\text{Exp}} - N_i^{\text{HRG}})^2}{(N_i^{\text{HRG}})^2}. \quad (12)$$

where N_i^{Exp} and N_i^{HRG} are the experimentally measured value and HRG model calculation of the i -th ratio yield, respectively with its uncertainty denoted by σ_i . For the experimental errors, we added the systematic errors of the measured ratios, while for the predicted error, we added the upper bound error of the model calculation. The sum runs over all ratios. The best-fitting chemical freeze-out parameters $\{T^{\text{FO}}, \mu_B^{\text{FO}}, \mu_S^{\text{FO}}, \mu_Q^{\text{FO}}\}$ are then extracted from this χ^2 -minimization procedure.

Figures 5 and 6 show the results of the thermal-fitting procedure applied to the π^-/π^+ , K^-/K^+ , \bar{p}/p , K^-/π^- , and \bar{p}/π^- hadron yield ratios for Ru+Ru and Zr+Zr, respectively. In both cases, red lines indicate the yield ratios produced by the hadron resonance gas with chemical freeze-out parameters $\{T^{\text{FO}}, \mu_B^{\text{FO}}, \mu_S^{\text{FO}}, \mu_Q^{\text{FO}}\}$ resulting from the fit to the yield ratios represented by closed circles. Preliminary STAR measurements [23] are shown as reference.

Parameter table.—The coefficients of the first-, second-, and third-order polynomial functions $p_m(Y_Q)$, used to

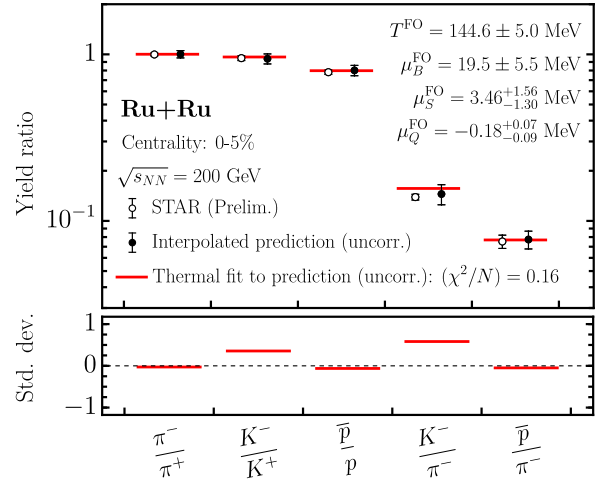


FIG. 5. Thermal fit of hadron yield ratios of identified charged particles for Ru+Ru at $\sqrt{s_{NN}} = 200$ GeV collisions obtained from interpolation of experimental values of other collision systems (see main text). The extracted yield ratios presented in Table III are represented by closed circles. Preliminary data from STAR measurements taken from Ref. [23] is represented by open circles and displayed only as reference.

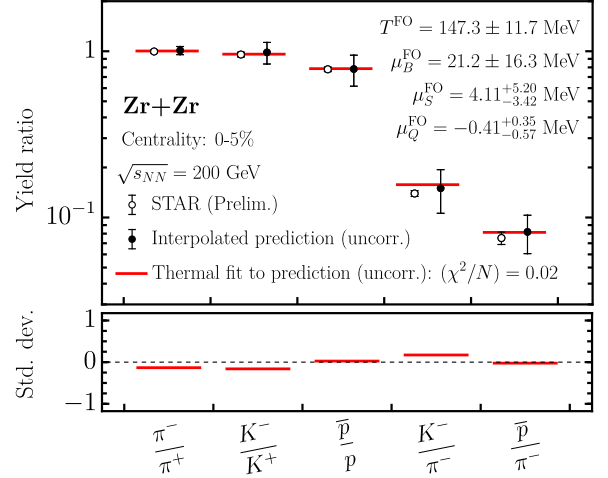


FIG. 6. Thermal fit of hadron yield ratios of identified charged particles for Zr+Zr at $\sqrt{s_{NN}} = 200$ GeV collisions obtained from interpolation of experimental values of other collision systems (see main text). The extracted yield ratios presented in Table III are represented by closed circles. Preliminary data from STAR measurements taken from Ref. [23] are shown as reference.

interpolate and extrapolate the hadron yield ratios as functions of Y_Q in Fig. 1, can, in principle, vary widely. In our analysis, different hadron yield ratios required different sets of parameters. We selected these parameters to cover the largest possible parameter space while keeping the computational effort reasonable. A summary of the chosen parameters is presented in Table IV.

Ratio/parameter	$a_{1,i}$	$\Delta_{1,i}$	$a_{2,i}$	$\Delta_{2,i}$	$a_{3,i}$	$\Delta_{3,i}$
π^-/π^+	[-4.0, 4.0]	0.001	[-50.0, 50.0]	0.50	[-50.0, 50.0]	1.0
K^-/K^+	[-10.0, 10.0]	0.010	[-150.0, 150.0]	0.10	[-100.0, 100.0]	0.5
\bar{p}/p	[-10.0, 10.0]	0.010	[-150.0, 150.0]	0.10	[-100.0, 100.0]	0.5
K^-/π^-	[-10.0, 10.0]	0.010	[-150.0, 150.0]	0.10	[-100.0, 100.0]	0.5
\bar{p}/π^-	[-10.0, 10.0]	0.010	[-150.0, 150.0]	0.05	[-100.0, 100.0]	0.5

TABLE IV. Ranges for coefficients $a_{m,i}$ and spacings $\Delta_{m,i}$ used for the estimation of all possible polynomials $p_m(Y_Q)$ (where $m = \{1, 2, 3\}$) that satisfy experimental data points and uncertainties for all hadron yield ratios considered. All coefficients of $p_m(Y_Q)$ have the same parameter range for fixed order, i.e., independently of $i = \{0, \dots, m\}$.